ARTICLES

nature cell biology

RhoA and microtubule dynamics control cell–basement membrane interaction in EMT during gastrulation

Yukiko Nakaya[1], Erike W. Sukowati[1], Yuping Wu[1] and Guojun Sheng[1,2]

Molecular and cellular mechanisms of epithelial–mesenchymal transition (EMT), crucial in development and pathogenesis, are still poorly understood. Here we provide evidence that distinct cellular steps of EMT occur sequentially during gastrulation. Basement membrane (BM) breakdown is the first recognizable step and is controlled by loss of basally localized RhoA activity and its activator neuroepithelial-transforming-protein-1 (Net1). Failure of RhoA downregulation during EMT leads to BM retention and reduction of its activity in normal epithelium leads to BM breakdown. We also show that this is in part mediated by RhoA-regulated basal microtubule stability. Microtubule disruption causes BM breakdown and its stabilization results in BM retention. We propose that loss of Net1 before EMT reduces basal RhoA activity and destabilizes basal microtubules, causing disruption of epithelial cell–BM interaction and subsequently, breakdown of the BM.

EMT is a complex process that requires the coordination of multiple cellular events, including disruption of epithelial cell–cell junctions, loss of apicobasal polarity, breakdown of cell–BM interaction and changes in cytoskeletal architecture[1]. Molecular studies have revealed that it is regulated by several major pathways[2–4]. Extensive crosstalk between these pathways has been documented both *in vitro* and *in vivo*[2,4,5]. However, it is unclear whether EMT is regulated as a single process or at the level of its individual cellular events. Cadherins, which can mediate differential adhesion, are commonly viewed as a central target[6–8]. The picture emerging from diverse EMT-related studies suggests that precise molecular and cellular control of EMT is complex and context-dependent[9]. Rho GTPases belong to a superfamily of small GTPases, which consists of 22 members in mammals[10]. Among its five major subfamilies, three (Rho-like, Cdc42-like and Rac-like) have been reported to function in EMT-related cellular events, such as cytoskeletal remodelling, microtubule dynamics, the maintenance of tight junctions and cadherin-mediated interactions[10–13].

The earliest EMT in development occurs during gastrulation, a process that generates mesoderm and endoderm from the ectoderm[14,15]. In amniotes, the majority of cells undergoing gastrulation EMT contribute to mesoderm[15,16]. Coordinated cell ingression during gastrulation is crucial for separating mesoderm-fated cells from adjacent non-ingressing neuroectoderm cells[17], and for generating anterior/posterior regionalization by controlling the timing of mesoderm formation[18]. Pan-mesoderm markers start to be expressed while precursor cells are still located in the epiblast, which consists of a single-cell-thick epithelial sheet and contains all ectoderm-fated cells, epithelial-shaped mesoderm precursor cells and pre-ingression mesoderm cells that may have lost some of their epithelial characteristics. Many mouse mutations causing gastrulation defects do not affect expression of pan-mesoderm markers, suggesting that mesoderm-fate specification and EMT are regulated independently. Moreover, it has been postulated that the individual cellular events of EMT during gastrulation may be under separate molecular controls[19]. A similar concept, termed EMT phenotypic modules[4] or intracellular crosstalk modules[20], has been proposed for the EMT process in general. Due to limitations of *in vivo* studies, such a concept has only recently started to be tested in amniotes.

In this study we have investigated the order and regulation of EMT cellular events during avian gastrulation. In particular, we show that controlled BM breakdown is a crucial component of, and the first recognizable step in, gastrulation EMT. In pre-EMT epiblast cells, the BM is maintained by basally localized RhoA activity, mediated by RhoGEF Net1. Loss of basal RhoA activity during EMT leads to disruption of cell–BM interaction and consequently to BM breakdown. We also provide evidence that basal microtubule stability has a crucial function in this process. Our data demonstrate an important role of BM regulation in an essential and evolutionarily conserved developmental process.

RESULTS

Mis-expression of RhoA causes EMT defects

RhoA-expressing cells fail to contribute properly to mesoderm lineages[21,22]. We investigated the timing of the defect with *in vivo* time-lapse imaging. Using gastrulation-stage chick embryos, we electroporated control green fluorescent protein (GFP) or wild-type RhoA+GFP at mid-streak level into mesoderm precursors located in the epiblast (Fig. 1a). In controls, 6 h after electroporation, most GFP-positive cells completed their ingression, giving rise to individually migrating

[1]Laboratory for Early Embryogenesis, RIKEN Center for Developmental Biology, Kobe, Hyogo 650-0047, Japan.
[2]Correspondence should be addressed to G.S. e-mail: (sheng@cdb.riken.jp)

Received 8 January 2008; accepted 23 April 2008; published online 15 June 2008; DOI: 10.1038/ncb1739

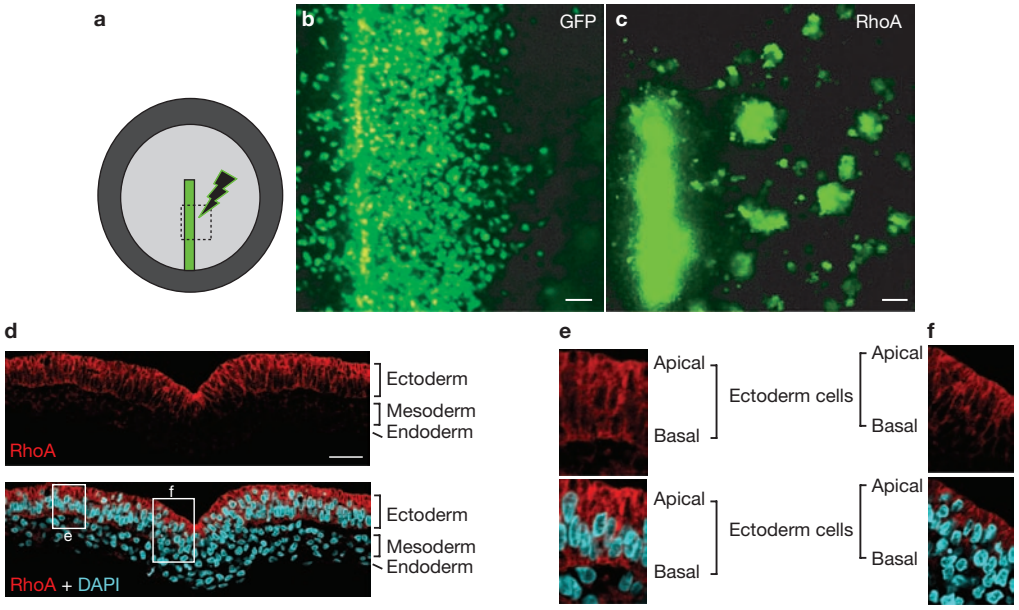

Figure 1 RhoA mis-expression causes EMT defects. (**a**) Schematic diagram of electroporated area in **b** and **c**. (**b**) GFP-expressing cells show normal ingression and migration. (**c**) RhoA+GFP-expressing cells show ingression and migration defects. (**d**) RhoA protein expression at HH4 embryo, sectioned through mid-streak level. Germ layers indicated on the right. Regions of magnified views in **e** and **f** indicated with white rectangles. (**e**) Lateral epiblast cells, showing both apical and basal RhoA. (**f**) Medial epiblast cells, lacking basal RhoA. Scale bars are 50 μm (**b**, **c**) and 30 μm (**d**).

mesoderm cells (Fig. 1b; Supplementary Information, Fig. S1, Movie 1). In contrast, many RhoA-expressing cells failed to complete EMT and accumulated in streak midline (Fig. 1c); those able to ingress formed aggregates (Fig. 1c; Supplementary Information, Fig. S1, Movie2). This suggests that RhoA has a role in the cellular events leading to mesoderm-cell ingression and early migration. Immunofluorescent staining showed that RhoA is expressed strongly in the epiblast, but is undetectable in the mesoderm (Fig. 1d). Within individual epiblast cells, we saw localized expression along the apicobasal axis. In medial cells, RhoA was only detected in the apical part (Fig. 1f), whereas both apical and basal expression was observed in cells lateral to the streak (Fig. 1e). This led us to investigate the significance of basal RhoA downregulation in gastrulation EMT.

BM breakdown is the first recognizable step of EMT

The temporal sequence of cellular events during gastrulation EMT has not been carefully investigated in amniotes. We first characterized expression patterns of several EMT-related markers: aPKC (apical), ZO-1 (tight junction), E-cadherin and N-cadherin (adherens junction) and fibronectin and laminin (BM). Both aPKC and ZO-1 (Fig. 2a, b) were expressed in all epiblast cells and were undetectable in mesoderm cells. E-cadherin (Fig. 2c) was expressed in epiblast and nascent mesoderm cells, with a gradual shift to N-cadherin in more lateral mesoderm cells (Fig. 2d). Fibronectin and laminin (Fig. 2e, f) were detected beneath the epiblast cells lateral to the streak. Their degradation was seen at a distance of 5–10 cells away from streak midline (Figs 2e, f). These data indicate that BM breakdown is the earliest cellular event leading to EMT during chick gastrulation. Tight junctions and apicobasal polarity are both maintained throughout epiblast cells and are lost immediately after ingression. In contrast to this sharp transition, change of adherens junction markers was gradual and did not correlate with ingression.

RhoA inhibits laminin breakdown in medial streak

We next analysed the effect of RhoA on these markers. RhoA mis-expression caused a marked retention of laminin in medial epiblast (Fig. 3c) and nascent mesoderm cells (Fig. 3b; Supplementary Information, Fig. S3a). Control GFP had no effect on laminin (Fig. 3a). No obvious change in aPKC, ZO-1 or adherens junction markers was observed with RhoA expression (Supplementary Information, Fig. S2a–c and data not shown). The effect on laminin is cell-autonomous, as retention was seen to be associated with individual newly ingressed mesoderm cells expressing RhoA (Fig. 3e). Lateral epiblast cells with exogenous RhoA did not upregulate normal laminin expression (Fig. 3d), and *in situ* analysis with *laminin γ1*, part of the laminin1-trimer, showed no detectable transcripts in mesoderm aggregates produced by RhoA (data not shown). This suggests that the effect of RhoA on laminin is due mainly to the failure of BM breakdown. Furthermore, analysis of integrin expression revealed that α6β1 is the major integrin isoform mediating the epiblast cell–BM interaction (Fig. 3f, g; Supplementary Information, Fig. S3b, d). Both chains are downregulated in medial epiblast cells during normal gastrulation (Fig. 3f, g; Supplementary Information, Fig. S3b, d) and mis-expression of RhoA caused retention of both in nascent mesoderm aggregates (Fig. 3h, i; Supplementary Information, Fig. S3c, e). This suggests that BM retention caused by RhoA is an indirect consequence of failure to disrupt integrin-mediated epiblast cell–BM interaction.

As the presence of RhoA protein may not reflect the distribution of active RhoA, we used eGFP–rGBD as a sensor for the active form of RhoA[23] to detect the subcellular distribution of its activity. eGFP–rGBD was electroporated into the lateral epiblast and embryos were cultured until the electroporated cells began to ingress (Fig. 3j; Supplementary Information, Fig. S4). In ingressed mesoderm cells, eGFP–rGBD was seen throughout the cytoplasm (Fig. 3j_1), indicating a lack of subcellular localization and consistent with the absence of RhoA protein in these cells. In

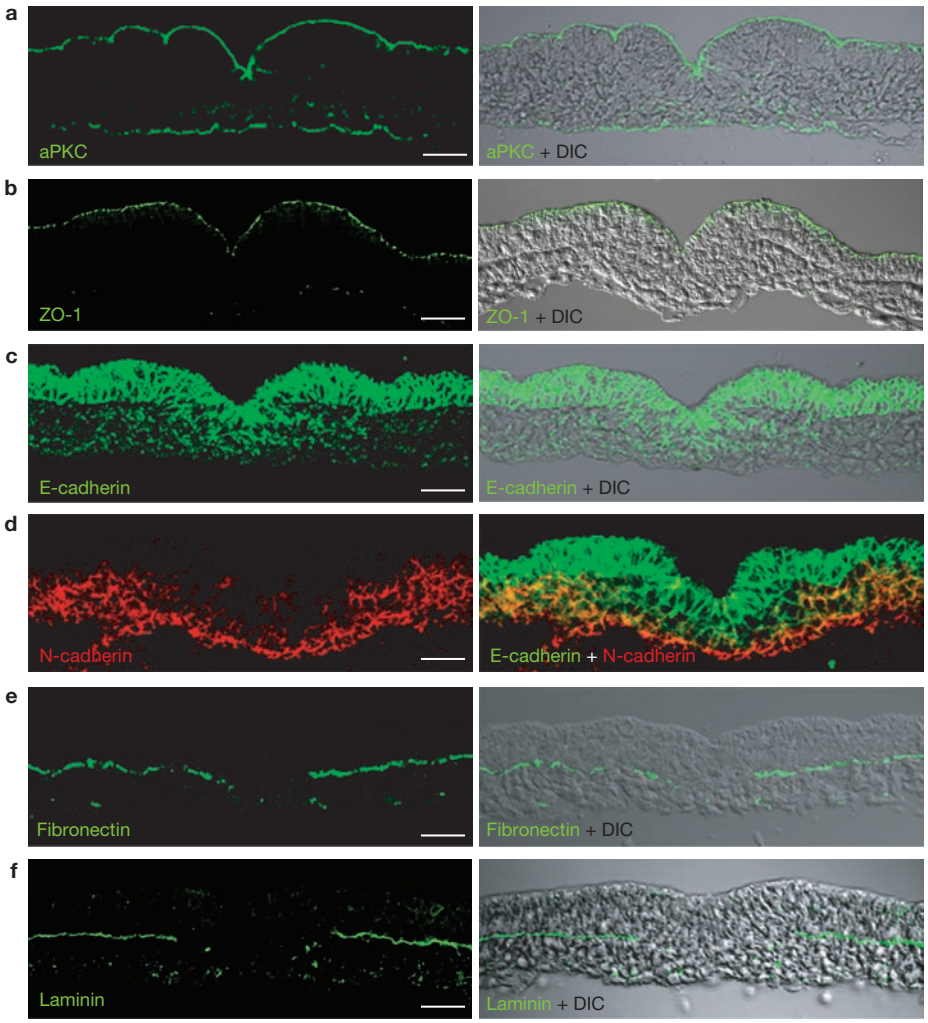

Figure 2 Expression of EMT-related markers. All panels show mid-streak-level section of stage HH4 embryo. (**a**) aPKC; (**b**) ZO-1; (**c**) E-cadherin; (**d**) N-cadherin; (**e**) fibronectin; (**f**) laminin. Right panel in **d** shows merged E-cadherin and N-cadherin. Scale bars are 30 μm.

the epiblast, we detected apical localization in all cells expressing eGFP–rGBD (Fig.3J$_{2-4}$), whereas basal eGFP–rGBD was observed only in more lateral cells (Fig. 3j$_4$, compared with 3j$_2$); this was most obvious in the transition region (Fig. 3j$_3$). Laminin co-staining revealed that the reduction in basal activity coincides with BM breakdown (Fig. 3j, green).

Net1, a RhoA GEF, is basally restricted in lateral epiblast and downregulated before EMT

RhoA cycles between the inactive GDP-bound and active GTP-bound states[10]. A family of GEFs catalyse the transition from the inactive to active state. We therefore investigated the role of RhoGEFs during gastrulation EMT. In a screen for genes differentially expressed in medial versus lateral epiblast (data not shown), we found that Net1, a RhoGEF, was specifically downregulated in medial epiblast cells. Net1 was first identified as an oncogene in human neuroepithelioma[24] and was shown to have RhoA-specific GEF activity[25–27].

The overall structure of chick Net1 is similar to that of other vertebrate Net1s (Fig. 4a). *In situ* analysis revealed a specific and dynamic pattern of *Net1* transcripts (Fig. 4b, c; Supplementary Information, Fig. S5a–d). At pre-streak stages, *Net1* expression was weak in the area pellucida (Supplementary Information, Fig. S5a); at gastrulation stages, expression became restricted to the future neuroepithelium (Fig. 4b, c; Supplementary Information, Fig. S5b). No expression was seen in the mesoderm at these stages (Fig. 4b$_1$, c$_{1,2}$). In medial epiblast cells, *Net1* transcripts were downregulated or absent (Fig. 4b$_1$, c$_2$). In lateral epiblast cells, its transcripts were seen to be restricted basally (Fig. 4b$_1$, c$_{1,2}$). To assess its protein localization, we generated a chick Net1 antibody and western blot analysis showed that it recognizes a specific band of expected size in cells transfected with a cNet1-expressing construct (Fig. 4d). Immunofluorescent staining revealed a basally restricted localizaton of Net1 protein (Fig. 4e), similar to that of integrin α6 (Fig. 4f), suggesting that Net1 is involved in regulating RhoA activity in the basal cortex or membrane of the epiblast cells. To test this, we generated an expression construct using mouse Net1 (ref. 28) and analysed its effect on laminin expression. Similarly to RhoA, Net1 mis-expression resulted in laminin retention in medial epiblast cells (Fig. 4g) and in mesoderm aggregation (data not shown).

Reducing RhoA activity causes premature BM breakdown

Prominent localization of RhoA in the apical cortex suggests that it has other roles in addition to BM maintenance. RhoA mis-expression,

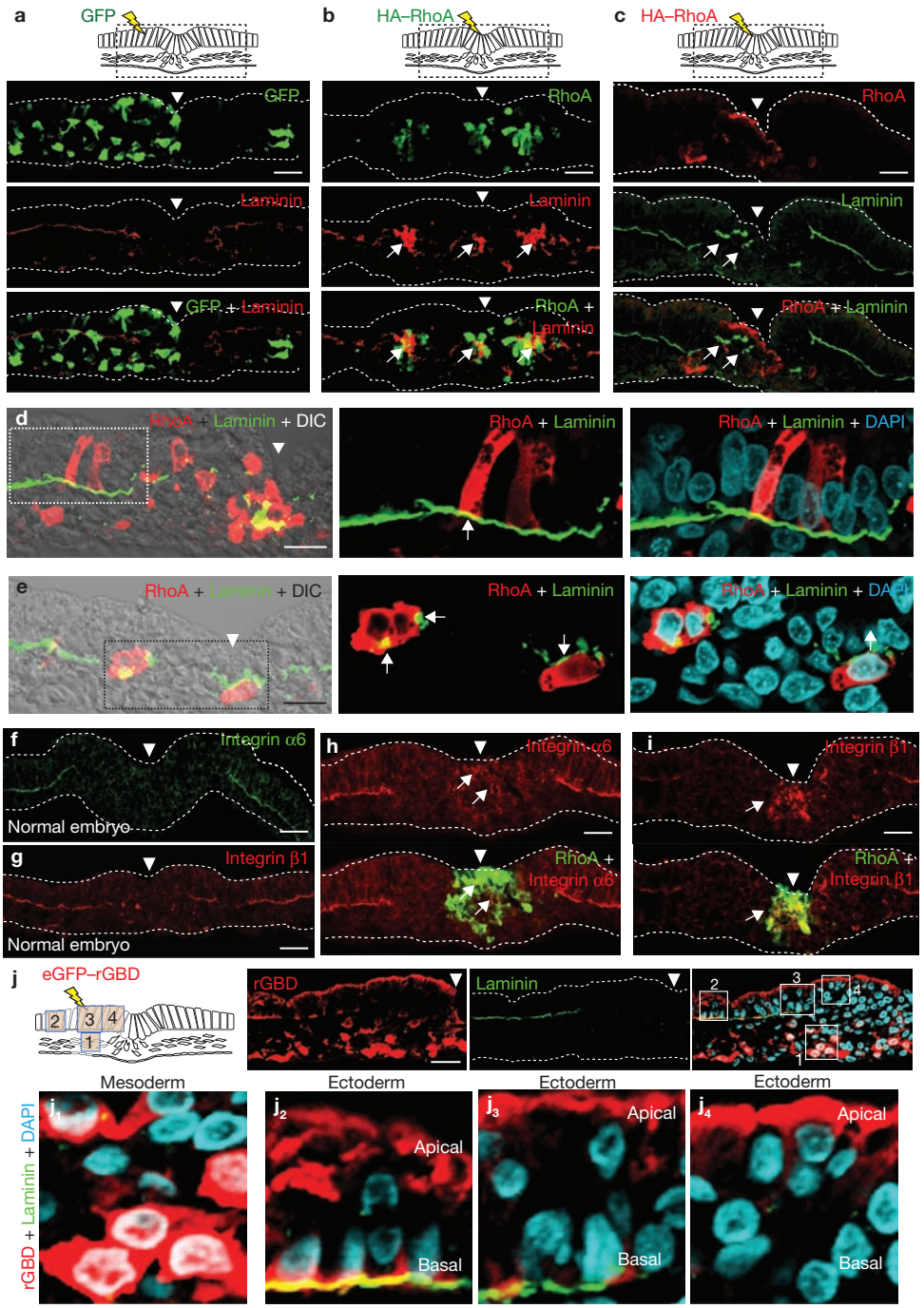

Figure 3 Effect of RhoA on laminin and distribution of active RhoA. (**a**–**c**) Electroporated regions are shown in the top panels (dotted rectangle). (**a**) GFP does not affect normal laminin expression. (**b**) RhoA causes cell aggregation with ectopic laminin (white arrows). (**c**) RhoA prevents laminin degradation in medial epiblast (white arrows). (**d**) Individual RhoA-expressing cells in the lateral epiblast have normal laminin levels. (**e**) Individual RhoA-expressing cells in medial streak region are seen associated with ectopic laminin (arrows; dotted rectangles in **d** and **e** are the regions magnified in the right panels. (**f**, **g**) Protein expression of integrin α6 (**f**) and β1 (**g**). (**h**, **i**) Ectopic RhoA induces ectopic α6 (**h**, arrows) and β1 (**i**, arrows) expression. (**j**) Localization of active RhoA shown with eGFP–rGBD. Magnified views of indicated areas shown in j_{1-4}. In mesoderm cells (j_1), eGFP–rGBD (red) is distributed throughout the cytoplasm. In lateral epiblast cells (j_2), eGFP–rGBD is seen in both apical and basal sides. Basal eGFP–rGBD colocalizes with laminin (green), seen as merged yellow colour. In epiblast cells undergoing BM degradation (j_3), loss of basal eGFP–rGBD coincides with loss of laminin. In medial epiblast cells (j_4), no basal eGFP–rGBD or laminin was detected. Apical localization of eGFP–rGBD is still prominent. Scale bars are 20 μm (**d**, **e**) and 30 μm (**a**–**c**, **f**–**j**). Arrowheads indicate streak midline.

however, had a marked effect only on BM markers. To confirm the role of basal RhoA in BM maintenance, we investigated the effect of reducing RhoA activity on gastrulation and laminin expression. We first used C3 exoenzyme, a potent Rho pathway inhibitor[29]. As described earlier, RhoA caused nascent mesoderm cells to form aggregates because of the failure in BM breakdown (Fig. 5a_1, arrows). This was rescued by

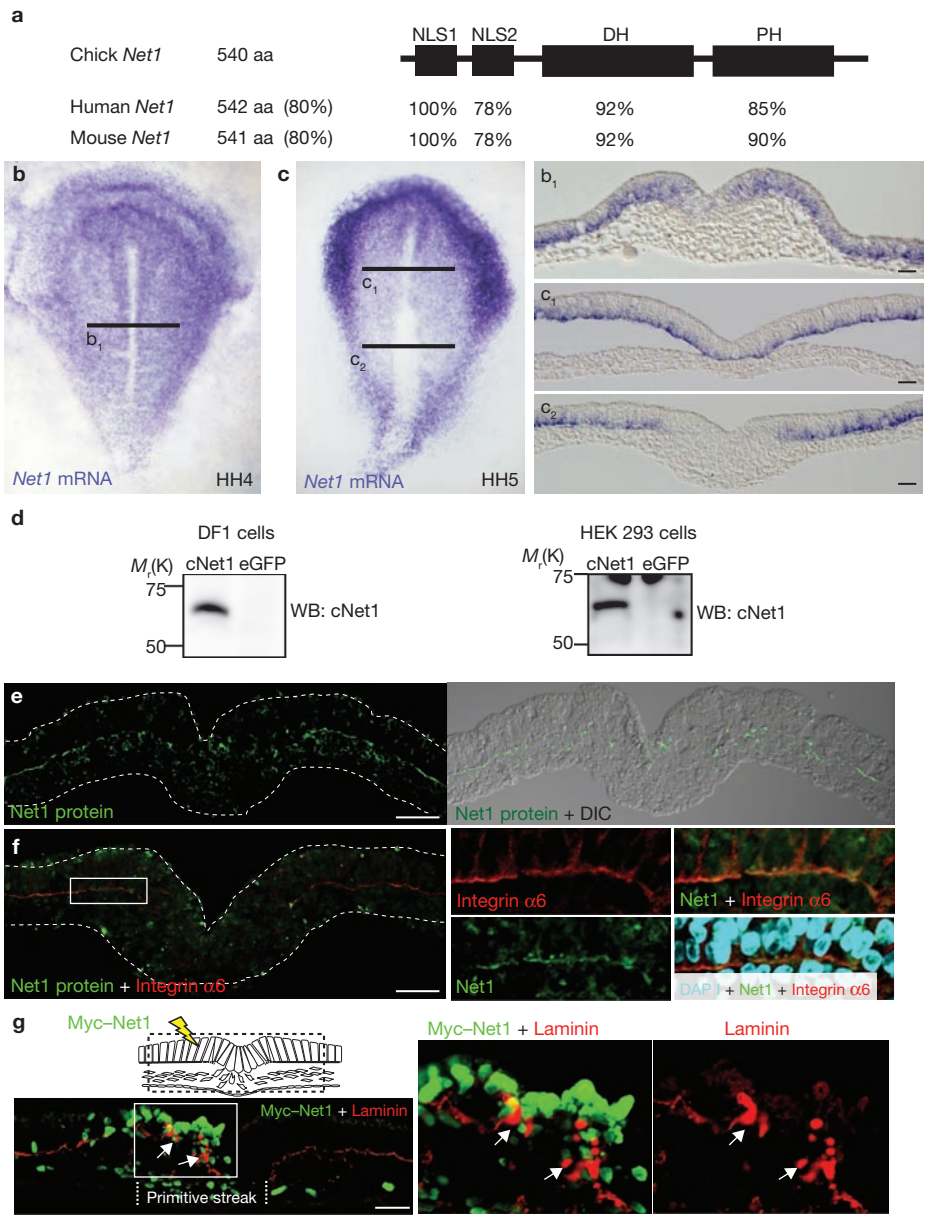

Figure 4 Net1 expression pattern and its effect on laminin. (**a**) Diagram of chick *Net1* and its homology to mammalian *Net1* (NLS: nuclear localization sequence; DH: Dbl homology domain; PH: pleckstrin homology domain). (**b**, **c**) Whole-mount *in situ* of *Net1* transcripts at stage HH4 (**b**) and HH5 (**c**). Black lines: section levels. (**d**) Specificity of anti-Net1 antibody shown with exogenously introduced cNet1 in DF1 (left) and HEK293 (right) cells. (**e**) Immunostaining with chick anti-Net1 antibody. (**f**) Co-staining of Net1 and integrin α6. (**g**) Mouse-Net1 protein expressed in medial epiblast cells retains laminin (arrows). Scale bars are 30 μm.

co-expression of C3 and RhoA (Fig. 5a$_2$, arrows). In contrast to RhoA-expressing cells (Fig. 3b), these cells did not have laminin (Fig. 5b, arrows; Supplementary Information, Fig. S3f). C3-expressing mesoderm cells migrated individually (Fig. 5a$_3$, arrows), although epiblast cell ingression was perturbed (Fig. 5a$_3$; Supplementary Information, Fig. S2d), possibly due to a marked effect of C3 on both apical and basal RhoA activities. In epiblast cells away from the streak, the effect of C3 on BM integrity was clearly seen (Supplementary Information, Fig. S2e), leading to ectopic EMT (Supplementary Information, Fig. S2e). These cells showed premature breakdown of the BM, and either ingressed as in normal EMT (white arrows) or egressed into the apical space above the epiblast (Supplementary Information, Fig. S2e, yellow arrows).

Because the effect of C3 may be broader than inhibiting only RhoA activity, we next used antisense morpholino oligonucleotides (MOs) against *RhoA* and *Net1* to reduce RhoA activity. Both *RhoA*- and *Net1*-MOs were able to specifically reduce transcript and protein levels (Supplementary Information, Fig. S6a–d for transcripts, Fig. S6e–j for proteins). Control MOs did not affect laminin expression (Fig. 5c). Cells receiving *RhoA-MOs* or *Net1-MOs* remained in the epiblast but showed premature breakdown of laminin (*RhoA-MOs*: 58% with $n = 79$ cells; *Net1-MOs*: 72% with $n = 78$) (Fig. 5d, e, arrows). A similar effect on BM breakdown was seen with a construct expressing dominant-negative RhoA (DN-RhoA; Supplementary Information, Fig. S5e). Additional *RhoA*- or *Net1*-specific MOs and their 5-mismatch controls confirmed the above observations

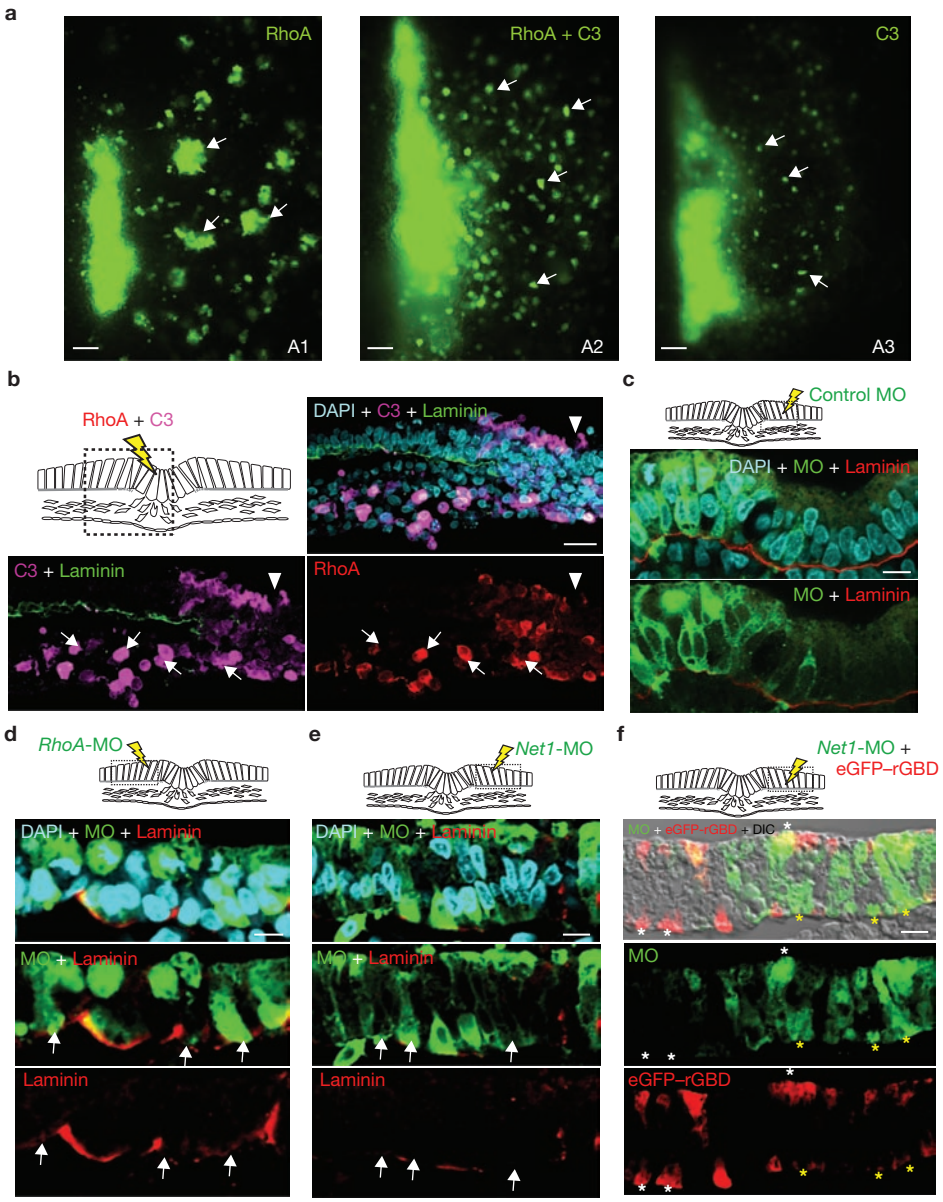

Figure 5 Inhibition of RhoA signalling causes premature BM breakdown and rescues mesoderm aggregation. Diagrams in **b**–**h** indicate regions shown in section. White arrowheads: midline. (**a**) C3 rescues RhoA-induced cell aggregation. RhoA alone causes mesoderm cell aggregation (**A1**, arrows); C3 rescues aggregation caused by RhoA (**A2**, arrows); C3 alone does not cause mesoderm cell aggregation (**A3**, arrows). (**b**) Section shows C3+RhoA-expressing cells do not form aggregates or express laminin (arrows). (**c**–**f**) Reducing RhoA activity by *RhoA* or *Net1* MOs causes laminin breakdown in lateral epiblast cells. (**c**): Control MOs do not affect laminin. (**d**): *RhoA*-MOs cause BM breakdown (arrows). (**e**) *Net1*-MOs cause BM breakdown (arrows). (**f**) *Net1* MOs reduce basal RhoA activity (yellow asterisks), whereas apical RhoA activity was not affected (white asterisks). Scale bars are 50 μm (**a**), 30 μm (**b**) and 10 μm (**c**–**f**).

(Supplementary Information, Fig. S6k, l). These additional MOs showed comparable efficiency in causing BM breakdown (*RhoA–TB2*: 72% $n = 87$; *RhoA–TB1+TB2*: 62% $n = 93$; *Net1–TB2+SB2*: 78% $n = 82$). The specificities of translation-block MOs were more clearly demonstrated in a *Xenopus laevis* assay system (Supplementary Information, Fig. S6k$_1$, l$_1$). Furthermore, confirming the basal specific activity of Net1 protein, *Net1*-MOs in epiblast cells resulted specifically reduced basal RhoA activity, as revealed by co-introduced eGFP–rGBD localization (59%, $n = 70$; Fig. 5f; yellow asterisks), whereas apical RhoA activity was not affected, with similar levels in cells that do or do not have MO present (white asterisks).

Nocodazole causes BM breakdown and taxol causes BM retention

Net1 is expressed and basally localized only in cells with basal RhoA activity (Fig. 4). We next investigated how this activity can maintain extracellular laminin. Data shown in Fig. 3f–i and Fig. 4e, f indicate that integrin-mediated cell–BM interaction may be a more direct target, possibly through RhoA regulation of actin cytoskeletal or microtubule dynamics[10] at the basal cortex of epiblast cells. HH4 embryos were treated with cytochalasin D or nocodazole to determine whether chemicals disrupting either actin filaments or microtubules, respectively, can affect laminin expression. Embryos treated

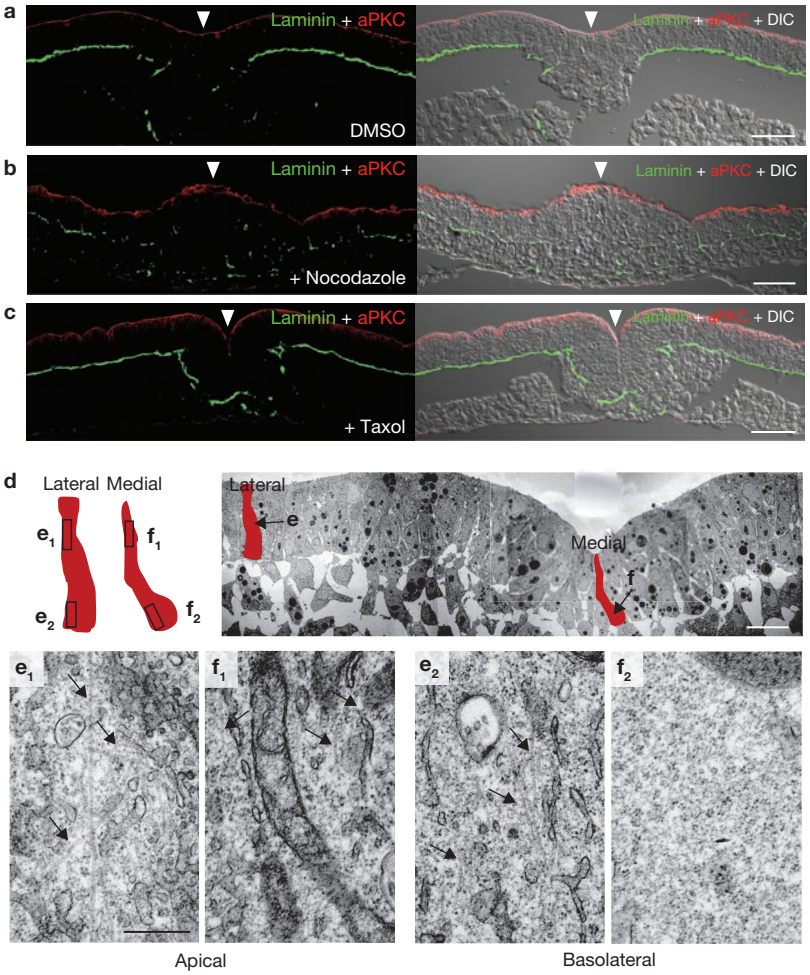

Figure 6 Effect of nocodazole and taxol on laminin and distribution of microtubules during EMT. (**a**–**c**) Section of HH4 embryo treated with DMSO (**a**), nocodazole (**b**) or taxol (**c**) for 2 h. White arrowheads: midline; green: laminin; red: aPKC. Nocodazole causes BM breakdown in lateral epiblast (**b**) and taxol causes BM retention in medial epiblast (**c**). (**d**) EM overview of HH4 embryo at mid-streak level. Locations of cells in **e** and **f** are indicated by arrows. (**e**) Lateral cell. (**f**) Medial cell. Regions shown in $\mathbf{e}_{1-2}$ and $\mathbf{f}_{1-2}$ are indicated in **d**. ($\mathbf{e}_1$, $\mathbf{f}_1$) Apical area. Arrows: microtubule. ($\mathbf{e}_2$, $\mathbf{f}_2$) Basal area. Microtubules (arrows) seen in lateral ($\mathbf{e}_2$), not in medial cell ($\mathbf{f}_2$). Scale bars are 30 μm (**a**–**c**), 20 μm (**d**) and 0.5μm (**e**).

with nocodazole showed prominent BM breakdown (Fig. 6b compared with Fig. 6a). Cytochalasin D treatment caused no obvious BM breakdown, but instead had a more prominent effect on apical integrity (data not shown). This indicates that basal RhoA activity may control BM maintenance by regulating microtubule stability at the basal side of epiblast cells. The effect of nocodazole, however, may be general and its effect on BM integrity secondary. We therefore tested the effect of taxol, a chemical that stabilizes dynamic microtubules. Taxol treatment had no effect on laminin expression in lateral epiblast cells, whereas in medial epiblast cells it caused prominent BM retention (Fig. 6c), suggesting that microtubule stability in epiblast cells is directly involved in BM maintenance.

Basal microtubule loss coincides with BM breakdown

If RhoA activity regulates microtubule stability in epiblast cells, we would expect destabilization of microtubules to be limited to the basal side of medial epiblast cells, as prominent apical RhoA protein and activity were observed in both lateral and medial epiblast cells (Figs 1d, 3j). To test this, we examined the abundance of microtubules in lateral and medial epiblast cells by electron microscopy (Fig. 6d, overview). In lateral cells (Fig. 6e), microtubules were seen throughout the cell along the apicobasal axis (Fig. $6e_{1,2}$). In medial cells (Fig. 6f), they were seen in apical regions with similar abundance, as in lateral cells (Fig. $6f_1$), but were rarely detectable in the basal or basolateral region (Fig. $6f_2$). This was confirmed by counting microtubules detectable under the electron microscope (Supplementary Information, Fig. S7j) and by immunohistochemical staining with antibodies against pan β-tubulin (Supplementary Information, Fig. S7a–f) and tyrosinated α-tubulin (Supplementary Information, Fig. S7g), strongly suggesting that destabilization of basal microtubules is important for initiating BM breakdown during EMT. Furthermore, antibodies against acetylated and detyrosinated α-tubulin, which are commonly thought to recognize more stable microtubules, showed a primarily apical staining throughout the epiblast (Supplementary Information, Fig. S7h, i), suggesting that basal and apical microtubules may have some intrinsic difference.

Modified tubulin at the basal cortex is a potential mediator in RhoA-regulated BM maintenance

Our data demonstrate the importance of both RhoA and microtubule dynamics in regulating epiblast cell–BM interaction but it is not clear

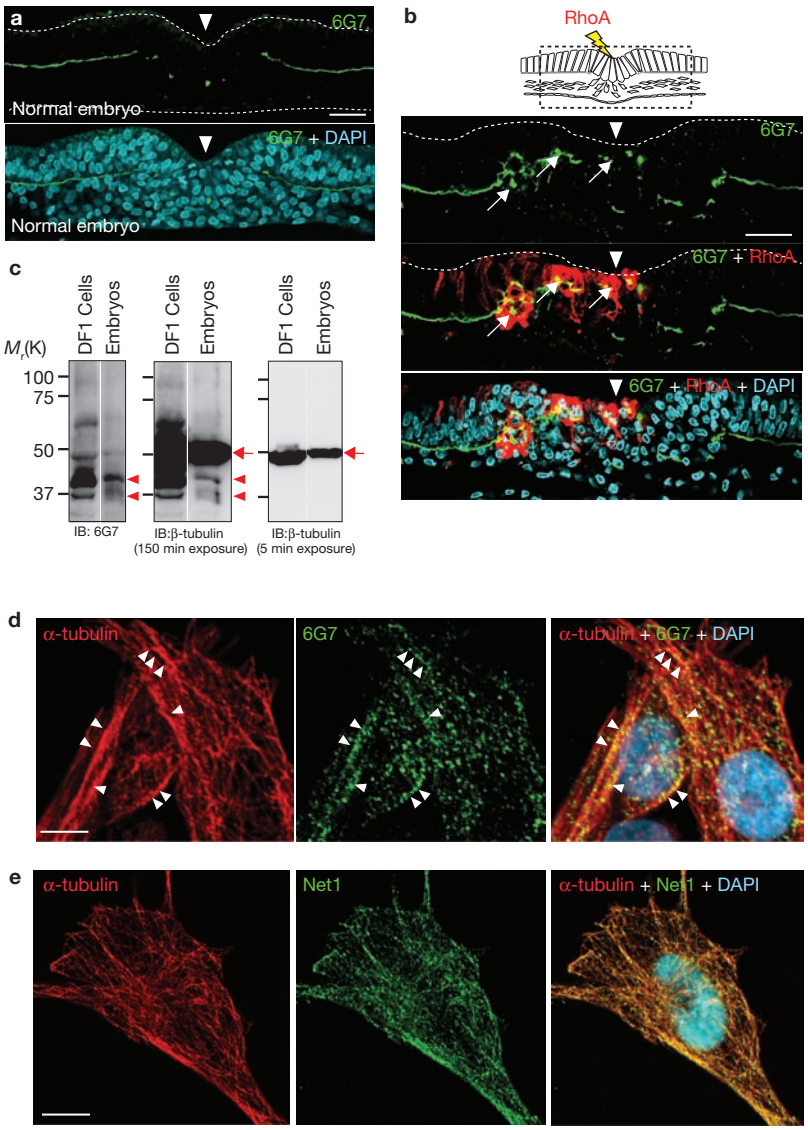

Figure 7 6G7 recognizes a modified β-tubulin localized to the basal cortex in lateral cells and absent in medial cells. (**a**) Section of HH4 embryo stained for 6G7. Arrowheads: midline. (**b**) RhoA mis-expression causes ectopic retention of 6G7 in medial epiblast (arrows). (**c**) Immunoblotting reveals that 6G7 recognizes several minor bands (one prominent minor band indicated by arrowheads), but not the major tubulin band (arrows) in pan-β-tubulin blot. The position of the minor band suggests a modified β-tubulin instead of a tubulin isoform. (**d**) Punctate localization of 6G7 to microtubules in DF1 cells. (**e**) Punctate localization of endogenous Net1 along microtubules in DF1 cells. Although 6G7 punctae are seen on microtubule tracts, Net1 punctae are seen more abundantly, and sometimes do not colocalize with microtubules. Scale bars are 30 μm (**a**, **b**) and 10 μm (**d**, **e**).

how they are linked. Microtubule stability can be a direct target for RhoA activity[30,31], and recent data suggest that Rho GTPases can regulate cell shape and polarity through modifying proteins associated with microtubule ends[32–35]. In addition, RhoGEFs have been reported to bind microtubules[36,37] and regulate microtubule-tip dynamics by controlling RhoA activity[37]. To find end-modifying proteins or modified forms of tubulins with localized expression in the epiblast, we found that 6G7, a chick β-tubulin antibody[38], recognizes an antigen with strikingly restricted expression (Fig. 7a). Immunoblotting showed that 6G7 recognizes a post-translationally modified β-tubulin (Fig. 7c). In lateral epiblast cells, 6G7 antigen was localized close to the basal cell membrane; whereas it was absent in medial epiblast cells. Moreover, when RhoA was mis-expressed in medial epiblast cells, 6G7 antigen was prominently retained (Fig. 7b, arrows). Although the precise nature of the modification awaits further study, immunostaining with cultured DF1 cells (chick fibroblast cells) revealed a punctate pattern of incorporation of 6G7-specific β-tubulin into microtubules (Fig. 7d). A similar pattern, although more abundant, was observed with endogenous Net1 along microtubules (Fig. 7e). In contrast, exogenously introduced Net1 was seen mainly in the nucleus (data not shown). These data suggest that special microtubule modifications at the basal cortex in normal epiblast cells may be an important target for Net1- and RhoA-regulated microtubule stabilization (Fig. 8).

DISCUSSION

EMT consists of a number of events that require precise coordination. In the context of gastrulation, we report here that these events take place in a spatially and temporally separable sequence (Figs 2, 8). Loss

of cell–BM interaction and breakdown of the BM take place first, when most cell–cell junctions are still intact. Loss of tight junctions occurs next, at the time when cells leave an integral epithelial sheet. The growth of early avian embryos requires epiblast tension generated by edge-cell migration in the area opaca and osmotic pressure build-up in the subgerminal cavity[39]. The maintenance of tight junctions in mesoderm precursor cells ensures epiblast integrity in the primitive streak. After ingression, cadherins shift gradually from epithelial to mesenchymal type. We suggest that this shift reflects the post-EMT migratory behaviour of most mesoderm cells. E-cadherin generally mediates more stable cell–cell adhesions in the epithelium, whereas N-cadherin mediates a more dynamic forming and breaking of cell–cell contacts[40].

During avian gastrulation, fibroblast growth factors (FGFs) induce BM breakdown poorly, despite being potent inducers of the mesoderm marker *brachyury*. However, another mesoderm inducer, Nodal, causes marked BM breakdown (data not shown). At present, we do not know how signals linked to the FGF, TGF-β, Wnt and Notch pathways, all crucial for proper gastrulation to take place, exert their influence on RhoA activity and its subcellular distribution. Initiation of expression in the epiblast of the mesoderm inducer Brachyury and EMT regulator Slug, both at the transcript and protein levels, precedes the initiation of BM breakdown (data not shown), suggesting that these transcription regulators may also regulate epiblast cell–BM interaction during EMT. Among Rho family GTPases, an obvious effect on gastrulation was only observed with RhoA mis-expression; whereas Rac and Cdc42, which have prominent roles during mesenchymal to epithelial transition in somitogenesis, do not perturb the gastrulation process when mis-expressed[41]. Chickens have three Rho-encoding genes, *rhoA*, *rhoB* and *rhoC*, sharing 83–93% identities at the protein level[42]. Although our study focuses on RhoA and null mutations of either *rhoB* or *rhoC* do not affect mouse development[43,44], some of our results may not be specific for RhoA and we cannot exclude the possible involvement of RhoB and/or RhoC.

Rho GTPases are important in multiple cellular events; however, studies linking specific cellular functions with localized Rho activity have emerged only recently[37,45–48]. Our data add to this growing list by revealing a link between basal RhoA activity and the maintenance of cell–BM interaction during gastrulation (Fig. 8). We also observed a strict basal localization of *Net1* transcripts and protein product, suggesting that basal RhoA activity is mediated by the localization of its activator. In cultured cells, mouse Net1 protein has a mainly nuclear localization; cytoplasmic localization is tightly controlled and correlates with its transforming ability[27]. RhoA, however, is also enriched on the apical side of ectoderm cells, possibly mediated by other apically localized GEFs. This seems to be the mechanism regulating apical RhoA activity during posterior spiracle formation in *Drosophila melanogaster* [47]. In this case, apical localization of RhoGEF64C and RhoGEF2, and basolateral localization of RhoGAP88C (crossveinless-c) control apical RhoA activity. Apical localization of *RhoGEF64C* transcripts was also reported[47], and together with our observations, suggests that *RhoGEF* mRNA localization is important in mediating Rho activity. Targeted transport of *RhoA* mRNA itself has also been reported to contribute to localized RhoA activity[48].

How does basal RhoA activity regulate cell–BM interaction? Here we provide evidence supporting the involvement of microtubules in this process. Immunohistochemistry and electron microscopy analyses

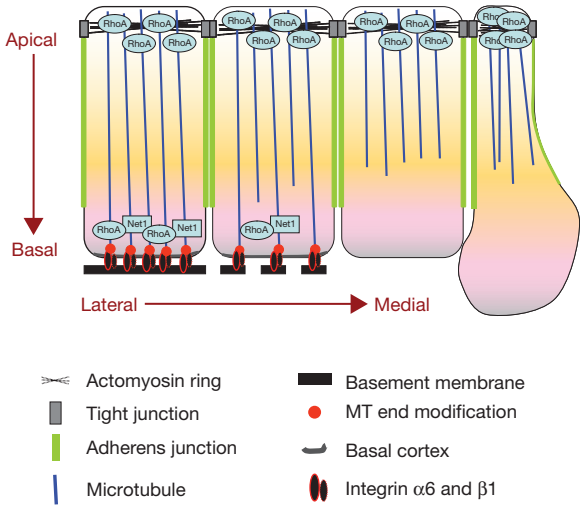

Figure 8 A model for the regulation of cell–BM interaction by basal RhoA activity and microtubule dynamics. The breakdown of BM precedes the loss of tight junctions and change in adherens junctions type. This is mediated by loss of basal Net1 and RhoA activity in medial epiblast cells. This results in disruption of basal microtubules and integrin-mediated epiblast cell–BM interaction and subsequently, breakdown of BM.

show that microtubules are rarely detected in the basal compartment of medial epiblast cells undergoing BM breakdown. In lateral epiblast cells, the dynamics of microtubules are different in apical (acetylated and detyrosinated tubulins; Supplementary Information, Fig. S7h, i) and basal (6G7; Fig. 7a) compartments. Treatment of embryos with chemicals affecting microtubule dynamics causes prominent effects on the BM. However, our analyses also show that nocodazole has a more immediate effect on basal RhoA activity and on basal integrin, than on BM integrity (Supplementary Information, Fig. S8a, b), suggesting that the epistatic relationship between basal RhoA and basal microtubules is not straightforward. On one hand, microtubules can be used to retain basal RhoA activity and the real target for active RhoA may be the basal cortical actin cytoskeleton. Loss of basal microtubules may be an indirect consequence of the loss of cell–BM interaction. On the other hand, RhoA activity can directly regulate basal microtubule stability; destabilization of these microtubules caused by loss of basal RhoA activity leads to the breakdown of cell–BM interaction. This hypothesis is supported by our observation that experimental destabilization of microtubules leads to rapid breakdown of the BM in normal epithelium, whereas actin destabilization does not cause obvious BM defects. Furthermore, RhoA-induced mesoderm cell aggregation can be rescued by nocodazole treatment (Supplementary Information, Fig. S8c-f). Our observations on the basal cortical localization of a specialized β-tubulin recognized by 6G7 and its retention by RhoA overexpression further support this model. A recent report, using cultured cells, showed that GEF–H1, is localized at the tips of cortical microtubules and functions in the regulation of microtubule dynamics through localized RhoA activation[37].

In summary, our data show that during the EMT process in gastrulation, basally localized RhoA activity and basal microtubule dynamics are essential for maintaining epiblast cell–BM interaction. Disruption of either one leads to the disruption of the other and subsequently to the loss of the BM. Further studies are required to understand how this is

regulated by multiple signalling pathways active during EMT and how the breakdown of epithelial cell–BM interaction is coordinated with the disruption of cell–cell junctions for the proper execution of EMT. □

METHODS

Embryology, imaging and immunohistochemistry. Fertilized hens' eggs were obtained from Shiroyama Farm (Kanagawa, Japan). Embryos were electroporated and cultured using standard methods[17]. All fluorescence microscopy images were taken with an Olympus FV1000, and fluorescent whole-mount images and non-fluorescent whole-mount or section images with Olympus BX51. For immunohistochemistry, the following primary antibodies were used: E-cadherin (1:500; BD transduction Lab, 610181), N-cadherin (1:1000; gift from M. Takeichi, RIKEN, Kobe, Japan), aPKC (1:60; Santa Cruz, sc-216), ZO-1 (1:100; Zymed, 40-2200), RhoA (1:100; LuLu51, gift from S. Yonemura[49]), fibronectin (1:100; $VA1_3$, DSHB), laminin (1:200; laminin-1, 3H11, DSHB; SIGMA, L9393), tyrosinated α-tubulin (1:100; Chemicon, MAB1864), acetylated α-tubulin (1:1000; Sigma, T6793), detyrosinated α-tubulin (1:100; Synaptic Systems, no. 302011), β-tubulin (1:100; 6G7, DSHB), HA-tag (1:100; 12CA5, Roche, 666 878), Myc-tag (1:300; MBL, 562; 9E10, Santa Cruz, sc-40), pan-β-tubulin (1:500; Sigma, T4026), Integrin α6 (1:100; P2C62C4, DSHB), Integrin β1 (1:300; Chemicon, MAB13443) and GFP (1:1000; Invitrogen, A-11122). Alexa Fluor secondary antibodies (1:300; Invitrogen) were used for multicolour detection. *Net1 in situ* analysis was performed using a standard protocol[17] with antisense digoxygenin probes against the last 0.5 kb of chick *Net1* (NCBI no. NM_001030648). Net1 antibody was generated against an N-terminal peptide (residues 19–35) by MBL (1:100, Nagoya, Japan). New cultures were treated with nocodazole (Sigma, M1404) at a concentration of 10 μg ml^{-1} dissolved in albumen, and taxol (Sigma, T7402) at 5 μg ml^{-1}. Cytochalasin D (Sigma, C8273) treatment was carried out at 4 μg ml^{-1}.

Expression constructs. DNA fragments were cloned into pCAGGS expression vector. Wild-type RhoA and DN-RhoA (T19N) with 3×HA tag were provided by Y. Takahashi (NAIST, Nara, Japan); cDNAs encoding mouse Net1 by J. Frost[28]; C3 by A. Hall (Memorial Sloan-Kettering Cancer Center, NY) and K. Kaibuchi (University of Nagoya, Japan). A tag of 6 Myc epitopes was added to Net1 and C3. eGFP–rGBD DNA was provided by W. Bement[45]. Fluorescein-tagged RhoA translation-block MO (RhoA–TB1; –22→+3 of translation initiation junction) 5′-CATAGCTGAAACACAAGAGGAC AAC-3′, E1I1 splicing-block MO (RhoA-SB1; –15→+10 of E1I1 junction) 5′-GTATA CATACCTGCTTTCCATCCAC-3′, Net1 translation-block MO (Net1-TB1; –1→+24 of translation initiation junction) 5′-CCCGAGCTCATCGTGAGC AACCATG-3′, I1E2 splicing-block MO (Net1-SB1; –13→+12 of I1E2 junction) 5′-ATTGCTTGGCTCCTGTAAATAAAGC-3′ and standard control MO were purchased from Genetools, and revealed with anti-fluorescein immunostaining (Invitrogen, no. A11090). Additional MOs used to confirm the specificities are: RhoA–TB2 (–54→–30 in 5′UTR) 5′-TCCTCCCATTGGA GCTTTTAATCGA-3′; 5-mismatch for RhoA–TB1 5′-CATCGCTCAAAGA CAAGACGAGAAC-3′; 5-mismatch for RhoA-TB2 5′-TCGTCGCATTGG ACCTTTAAATGGA-3′; 5-mismatch for RhoA–SB1 5′-GTAAACATAGCT CCTTTCGATCGAC-3′; Net1–TB2 (–6→+18 of translation initiation junction) 5′-CTCATCGTGAGCAACCATGGCGAA-3′; Net1–SB2 (–5→+20 of I1E2 junction) 5′-ACCCGTTTATTGCTTGGCTCCTGTA-3′; 5-mismatch for Net1 TB1 5′-CCGGACCTCATCCTGAGGAACGATG-3′; 5-mismatch for Net1 SB1 5′-ATTCCTTCGCTGCTCTAAATAATGC-3′; 5-mismatch for Net1–TB2 5′-CTGATCCTGAGCAACGATCGCCAA-3′; 5-mismatch for Net1–SB2 5′-ACACGTTTATTCCTTCGCTGCTCTA-3′. Specificity test of translation-block MOs in *Xenopus* were carried out according to a published protocol[50]. Briefly, 5′UTR region of cRhoA (–60→–1) and translation initiation junction region of cNet1 (–10→+24) were cloned in front of mCherry using pCS2 vector. *In vitro* transcribed mRNA (10 pg per cell for *Net1-mCherry*; 40 pg per cell for *RhoA-mCherry*) and indicated MOs (12.5 ng per cell for Net1 TB and 25 ng per cell for RhoA TB) were injected into four animal blastomeres at 8-cell stage. Animal cap explants were prepared at mid-blastula stage and collected at early gastrula, following by western blot analysis using an anti-DsRed antibody (Clontech, no. 32496). Net1 sequences used for phylogenetic comparison have following NCBI accession numbers: NM_001030648 (chick), BC004699 (mouse) and BC010285 (human).

Cell culture. DF1 chicken fibroblast cells were used for 6G7, Net1 and α-tubulin staining. DF1 and HEK293 cells were used for Net1 western blot analysis. Standard protocols were used for cell culture and transfection.

Electron microscopy. Electron microscopy studies were performed in the EM facility of RIKEN CDB with the help of S. Yonemura from the Laboratory for Cellular Morphogenesis. Samples were fixed with 2% fresh formaldehyde and 2.5% glutaraldehyde in 0.1 M cacodylate buffer (pH 7.3) for 2 h at room temperature and then post-fixed with 1% OsO_4 in the same buffer for 2 h on ice. They were rinsed with water, stained with 0.5% uranyl acetate overnight at room temperature, dehydrated with ethanol and embedded in Polybed 812 (Polyscience). Ultra-thin sections were cut, double-stained with uranyl acetate and lead citrate, and then examined with a JEM 1010 transmission electron microscope (JEOL) operated at an accelerating voltage of 100 kV.

Note: Supplementary Information is available on the Nature Cell Biology website.

ACKNOWLEDGEMENTS

We thank Fujio Toki for the initial analyses of fibronectin, laminin and 6G7; Yoshiko Takahashi for bringing the phenotype of RhoA cells to our attention; Kathy Joubin for sharing Net1 information; Cantas Alev for generating the *Net1* probe; Shigenobu Yonemura and Kazuyo Misaki for help with EM; Masatoshi Takeichi, Yoshiko Takahashi, William Bement, Jeffrey Frost, Alan Hall, Kozo Kaibuchi and Shigenobu Yonemura for sharing reagents; Noriaki Sasai and Yoshiki Sasai for help with *Xenopus* experiments. Claudio Stern, Donald Newgreen, Kozo Kaibuchi, Masatoshi Takeichi, Fumio Matsuzaki, Shigeo Hayashi and Shigenobu Yonemura for critical comments on the manuscript.

AUTHOR CONTRIBUTIONS

Y.N. and G.S. designed the experiments and analysed the data; Y.N, E.W.S. and Y.W. performed the experiments; G.S wrote the manuscript.

COMPETING FINANCIAL INTERESTS

The authors declare no competing financial interests.

Published online at http://www.nature.com/naturecellbiology/
Reprints and permissions information is available online at http://npg.nature.com/reprintsandpermissions/

1. Hay, E. D. An overview of epithelio–mesenchymal transformation. *Acta Anat. (Basel)* **154,** 8–20 (1995).
2. Huber, M. A., Kraut, N. & Beug, H. Molecular requirements for epithelial–mesenchymal transition during tumor progression. *Curr. Opin. Cell Biol.* **17,** 548–558 (2005).
3. Thiery, J. P. Epithelial–mesenchymal transitions in development and pathologies. *Curr. Opin. Cell Biol.* **15,** 740–746 (2003).
4. Zavadil, J. & Bottinger, E. P. TGF-β and epithelial-to-mesenchymal transitions. *Oncogene* **24,** 5764–5774 (2005).
5. Thiery, J. P. & Sleeman, J. P. Complex networks orchestrate epithelial–mesenchymal transitions. *Nature Rev. Mol. Cell Biol.* **7,** 131–142 (2006).
6. Hatta, K. & Takeichi, M. Expression of N-cadherin adhesion molecules associated with early morphogenetic events in chick development. *Nature* **320,** 447–449 (1986).
7. Zohn, I. E. *et al.* p38 and a p38-interacting protein are critical for downregulation of E-cadherin during mouse gastrulation. *Cell* **125,** 957–969 (2006).
8. Cano, A. *et al.* The transcription factor snail controls epithelial–mesenchymal transitions by repressing E-cadherin expression. *Nature Cell Biol.* **2,** 76–83 (2000).
9. Lee, J. M., Dedhar, S., Kalluri, R. & Thompson, E. W. The epithelial–mesenchymal transition: new insights in signaling, development, and disease. *J. Cell Biol.* **172,** 973–981 (2006).
10. Jaffe, A. B. & Hall, A. Rho GTPases: biochemistry and biology. *Annu. Rev. Cell Dev. Biol.* **21,** 247–269 (2005).
11. Fukata, M. & Kaibuchi, K. Rho-family GTPases in cadherin-mediated cell–cell adhesion. *Nature Rev. Mol. Cell Biol.* **2,** 887–897 (2001).
12. Van Aelst, L. & Symons, M. Role of Rho family GTPases in epithelial morphogenesis. *Genes Dev.* **16,** 1032–1054 (2002).
13. Ozdamar, B. *et al.* Regulation of the polarity protein Par6 by TGFbeta receptors controls epithelial cell plasticity. *Science* **307,** 1603–1609 (2005).
14. Keller, R. Cell migration during gastrulation. *Curr. Opin. Cell Biol.* **17,** 533–541 (2005).
15. Stern, C. D. *Gastrulation: from cells to embryo* (Cold Spring Harbor Laboratory Press New York, 2004).
16. Tam, P. P. & Behringer, R. R. Mouse gastrulation: the formation of a mammalian body plan. *Mech. Dev.* **68,** 3–25 (1997).
17. Sheng, G., dos Reis, M. & Stern, C. D. Churchill, a zinc finger transcriptional activator, regulates the transition between gastrulation and neurulation. *Cell* **115,** 603–613 (2003).
18. Iimura, T. & Pourquie, O. Collinear activation of Hoxb genes during gastrulation is linked to mesoderm cell ingression. *Nature* **442,** 568–571 (2006).
19. Gustafson, T. & Wolpert, L. Studies on the cellular basis of morphogenesis in the sea urchin embryo. Gastrulation in vegetalized larvae. *Exp. Cell Res.* **22,** 437–449 (1961).

20. Newgreen, D. F. & Minichiello, J. Control of epitheliomesenchymal transformation. I. Events in the onset of neural crest cell migration are separable and inducible by protein kinase inhibitors. *Dev. Biol.* **170,** 91–101 (1995).
21. Watanabe, T. *et al.* Tet-on inducible system combined with *in ovo* electroporation dissects multiple roles of genes in somitogenesis of chicken embryos. *Dev. Biol.* **305,** 625–636 (2007).
22. Fuse, T. *et al.* Conditional activation of RhoA suppresses the epithelial to mesenchymal transition at the primitive streak during mouse gastrulation. *Biochem. Biophys. Res. Commun.* **318,** 665–672 (2004).
23. Benink, H. A. & Bement, W. M. Concentric zones of active RhoA and Cdc42 around single cell wounds. *J. Cell Biol.* **168,** 429–439 (2005).
24. Chan, A. M., Takai, S., Yamada, K. & Miki, T. Isolation of a novel oncogene, NET1, from neuroepithelioma cells by expression cDNA cloning. *Oncogene* **12,** 1259–1266 (1996).
25. Alberts, A. S. & Treisman, R. Activation of RhoA and SAPK/JNK signalling pathways by the RhoA-specific exchange factor mNET1. *EMBO J.* **17,** 4075–4085 (1998).
26. Miyakoshi, A., Ueno, N. & Kinoshita, N. Rho guanine nucleotide exchange factor xNET1 implicated in gastrulation movements during *Xenopus* development. *Differentiation* **72,** 48–55 (2004).
27. Schmidt, A. & Hall, A. The Rho exchange factor Net1 is regulated by nuclear sequestration. *J. Biol. Chem.* **277,** 14581–14588 (2002).
28. Qin, H. *et al.* Characterization of the biochemical and transforming properties of the neuroepithelial transforming protein 1. *J. Biol. Chem.* **280,** 7603–7613 (2005).
29. Aktories, K., Braun, U., Rosener, S., Just, I. & Hall, A. The rho gene product expressed in *E. coli* is a substrate of botulinum ADP-ribosyltransferase C3. *Biochem. Biophys. Res. Commun.* **158,** 209–213 (1989).
30. Fukata, Y. *et al.* CRMP-2 binds to tubulin heterodimers to promote microtubule assembly. *Nature Cell Biol.* **4,** 583–591 (2002).
31. Palazzo, A. F., Cook, T. A., Alberts, A. S. & Gundersen, G. G. mDia mediates Rho-regulated formation and orientation of stable microtubules. *Nature Cell Biol.* **3,** 723–729 (2001).
32. Fukata, M. *et al.* Rac1 and Cdc42 capture microtubules through IQGAP1 and CLIP-170. *Cell* **109,** 873–85 (2002).
33. Lansbergen, G. *et al.* CLASPs attach microtubule plus ends to the cell cortex through a complex with LL5β. *Dev. Cell* **11,** 21–32 (2006).
34. Mimori-Kiyosue, Y. *et al.* CLASP1 and CLASP2 bind to EB1 and regulate microtubule plus-end dynamics at the cell cortex. *J. Cell Biol.* **168,** 141–153 (2005).
35. Wen, Y. *et al.* EB1 and APC bind to mDia to stabilize microtubules downstream of Rho and promote cell migration. *Nature Cell Biol.* **6,** 820–830 (2004).
36. van Horck, F. P., Ahmadian, M. R., Haeusler, L. C., Moolenaar, W. H. & Kranenburg, O. Characterization of p190RhoGEF, a RhoA-specific guanine nucleotide exchange factor that interacts with microtubules. *J. Biol. Chem.* **276,** 4948–4956 (2001).
37. Birkenfeld, J. *et al.* GEF–H1 Modulates localized RhoA activation during cytokinesis under the control of mitotic kinases. *Dev. Cell* **12,** 699–712 (2007).
38. Halfter, W., Dong, S., Yip, Y. P., Willem, M. & Mayer, U. A critical function of the pial basement membrane in cortical histogenesis. *J. Neurosci.* **22,** 6029–6040 (2002).
39. Stern, C. D., Manning, S. & Gillespie, J. I. Fluid transport across the epiblast of the early chick embryo. *J. Embryol. Exp. Morphol.* **88,** 365–384 (1985).
40. Gumbiner, B. M. Regulation of cadherin-mediated adhesion in morphogenesis. *Nature Rev. Mol. Cell Biol.* **6,** 622–634 (2005).
41. Nakaya, Y., Kuroda, S., Katagiri, Y. T., Kaibuchi, K. & Takahashi, Y. Mesenchymal–epithelial transition during somitic segmentation is regulated by differential roles of Cdc42 and Rac1. *Dev. Cell* **7,** 425–438 (2004).
42. Liu, J. P. & Jessell, T. M. A role for rhoB in the delamination of neural crest cells from the dorsal neural tube. *Development* **125,** 5055–5067 (1998).
43. Liu, A. X., Rane, N., Liu, J. P. & Prendergast, G. C. RhoB is dispensable for mouse development, but it modifies susceptibility to tumor formation as well as cell adhesion and growth factor signaling in transformed cells. *Mol. Cell Biol.* **21,** 6906–6912 (2001).
44. Hakem, A. *et al.* RhoC is dispensable for embryogenesis and tumor initiation but essential for metastasis. *Genes Dev.* **19,** 1974–1979 (2005).
45. Bement, W. M., Benink, H. A. & von Dassow, G. A microtubule-dependent zone of active RhoA during cleavage plane specification. *J. Cell Biol.* **170,** 91–101 (2005).
46. Pertz, O., Hodgson, L., Klemke, R. L. & Hahn, K. M. Spatiotemporal dynamics of RhoA activity in migrating cells. *Nature* **440,** 1069–1072 (2006).
47. Simoes, S. *et al.* Compartmentalisation of Rho regulators directs cell invagination during tissue morphogenesis. *Development* **133,** 4257–4267 (2006).
48. Wu, K. Y. *et al.* Local translation of RhoA regulates growth cone collapse. *Nature* **436,** 1020–1024 (2005).
49. Yonemura, S., Hirao-Minakuchi, K. & Nishimura, Y. Rho localization in cells and tissues. *Exp. Cell Res.* **295,** 300–314 (2004).
50. Sasai, N., Nakazawa, Y., Haraguchi, T. & Sasai, Y. The neurotrophin-receptor-related protein NRH1 is essential for convergent extension movements. *Nature Cell Biol.* **6,** 741–748 (2004).

nature cell biology

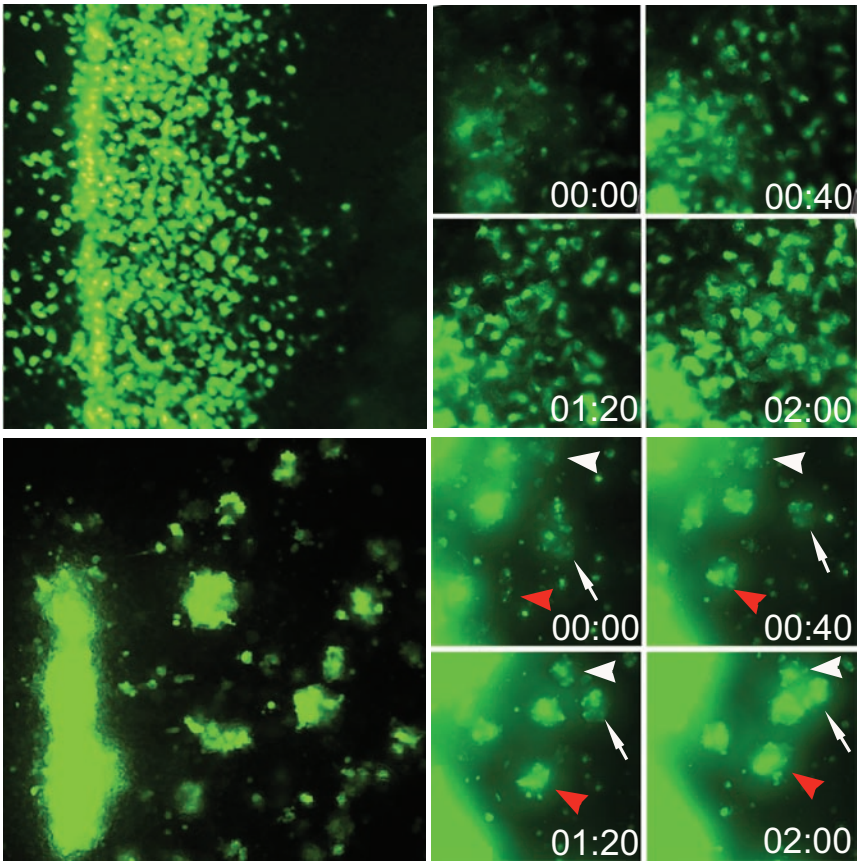

Figure S1 Time-lapse images of Fig.1b (top) and Fig.1c (bottom), showing the formation of aggregates (arrows and arrowheads) in RhoA+GFP-expressing embryo. Total duration: 2 hours.

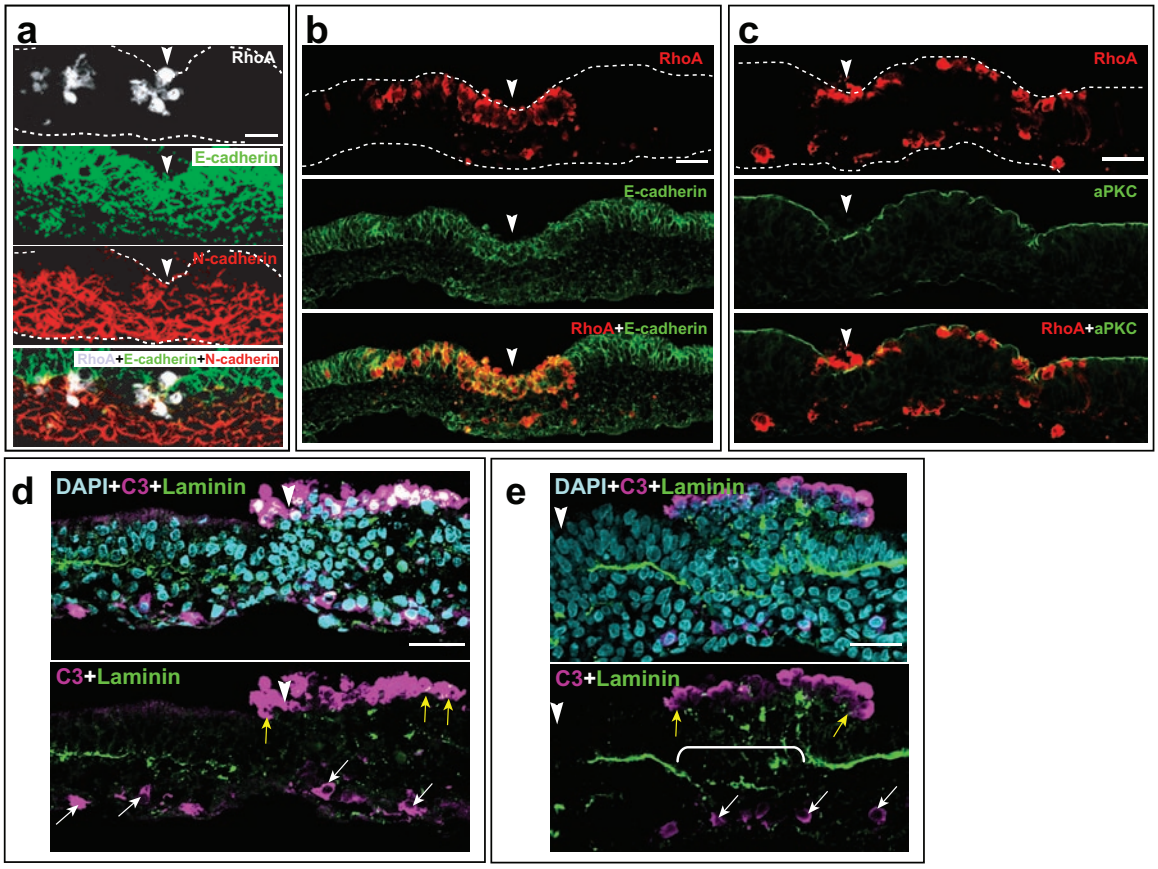

Figure S2 a-c: RhoA mis-expression does not cause obvious effect on Cadherins or aPKC. RhoA does not affect E-cadherin or N-cadherin expression in mesoderm cell aggregates (**a**), or E-cadherin in epiblast cells (**b**). RhoA does not affect aPKC expression in epiblast cells (**c**). **d,e:** Effect of C3 on epiblast and mesoderm cells. C3-expressing mesoderm cells do not form aggregates or express Laminin (white arrows in **d**). Some cells extruded apically are also Laminin negative (yellow arrows in **d**). C3 in lateral epiblast causes premature BM-breakdown and ectopic "EMT" (bracket in **e**). Some cells ingress into mesoderm layer (white arrows in **e**), others egress from epiblast (yellow arrows in **e**). None expresses Laminin. Scale bar: 30 μm.

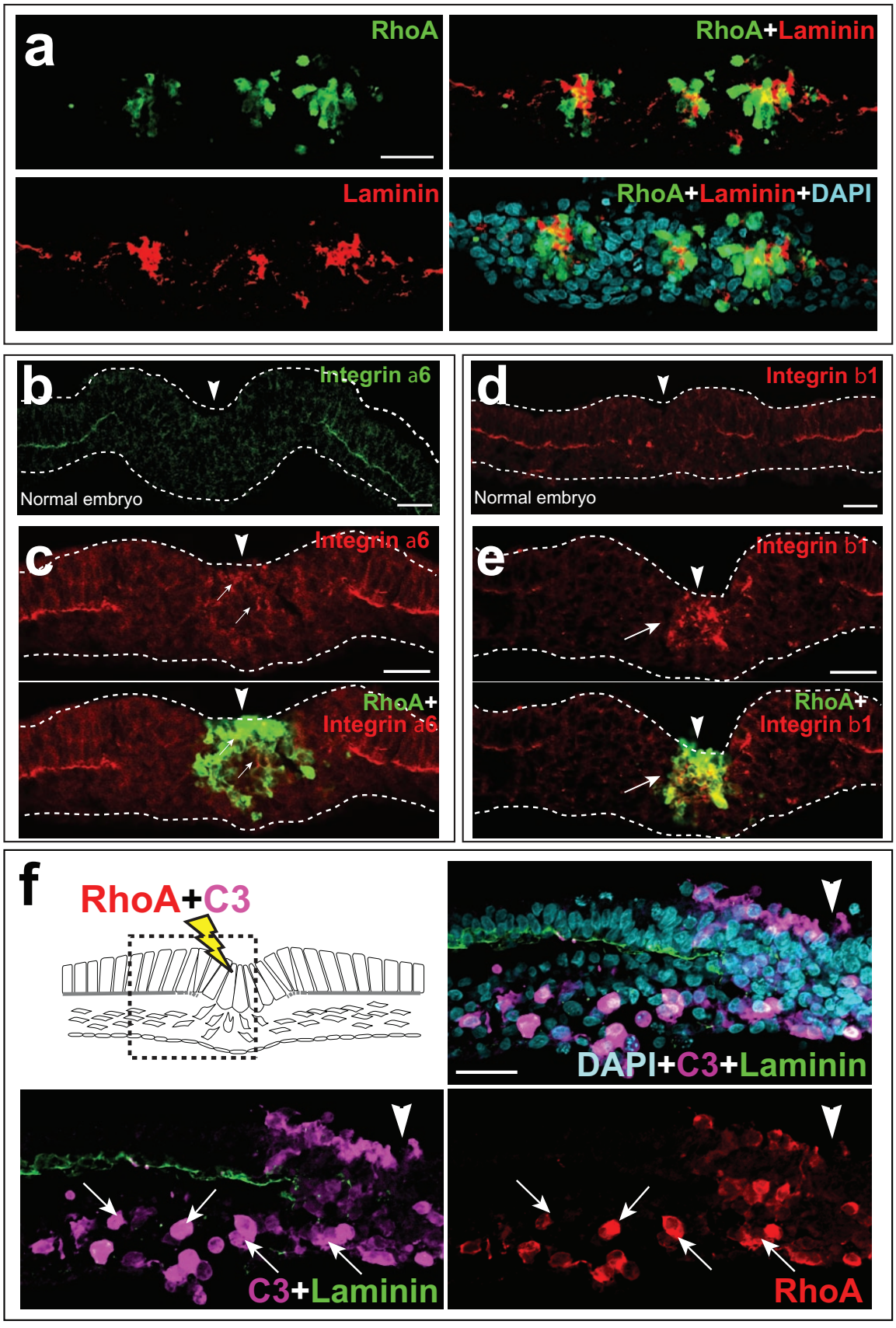

Figure S3 a: Magnified view of panels in Fig.3b. **b-e:** Magnified view of panels in Fig.3**f-i**. **f:** Magnified view of panels in Fig.5**b**. Scale bar: 30 μm.

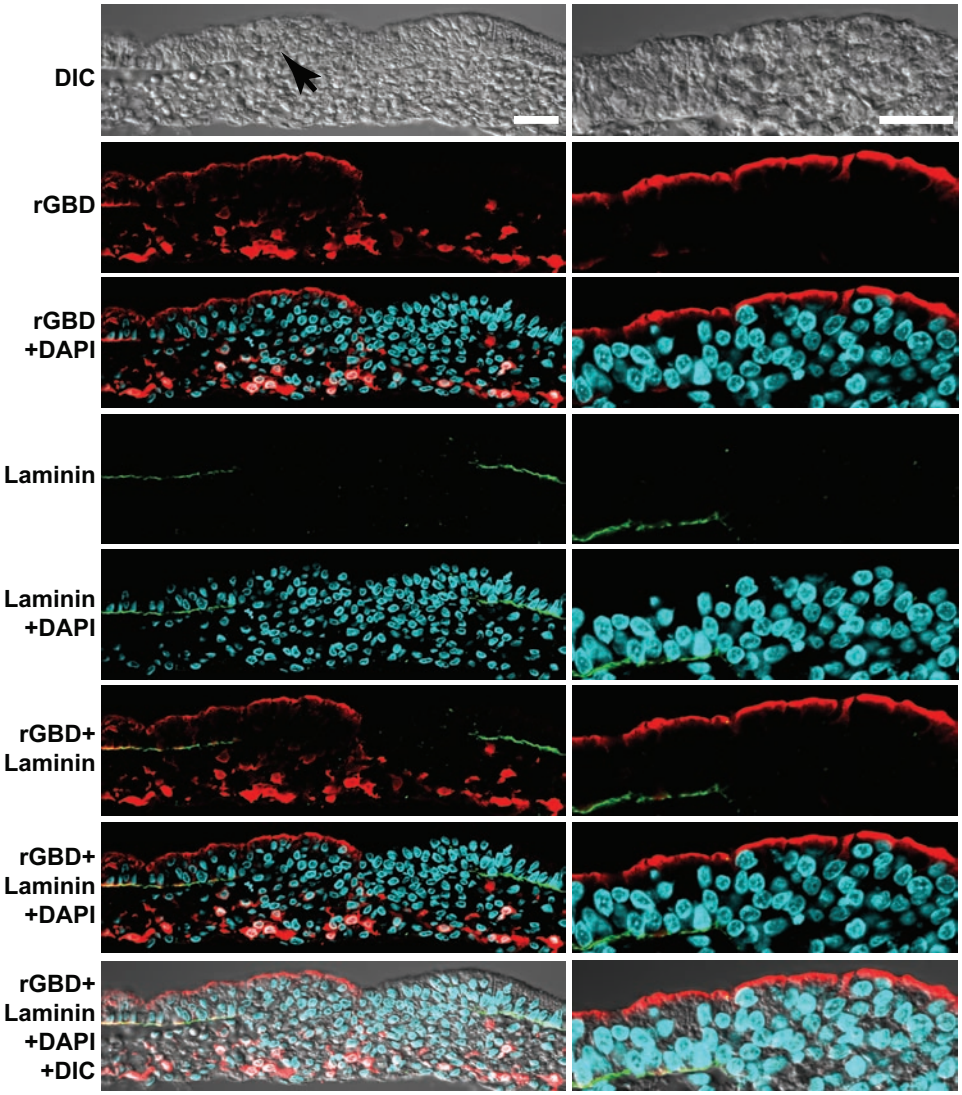

Figure S4 Left panels: images in Fig.3j shown with wider field of view in various overlay combinations. Right panels: magnified view of indicated area on left (arrow in DIC). Scale bar: 30 μm.

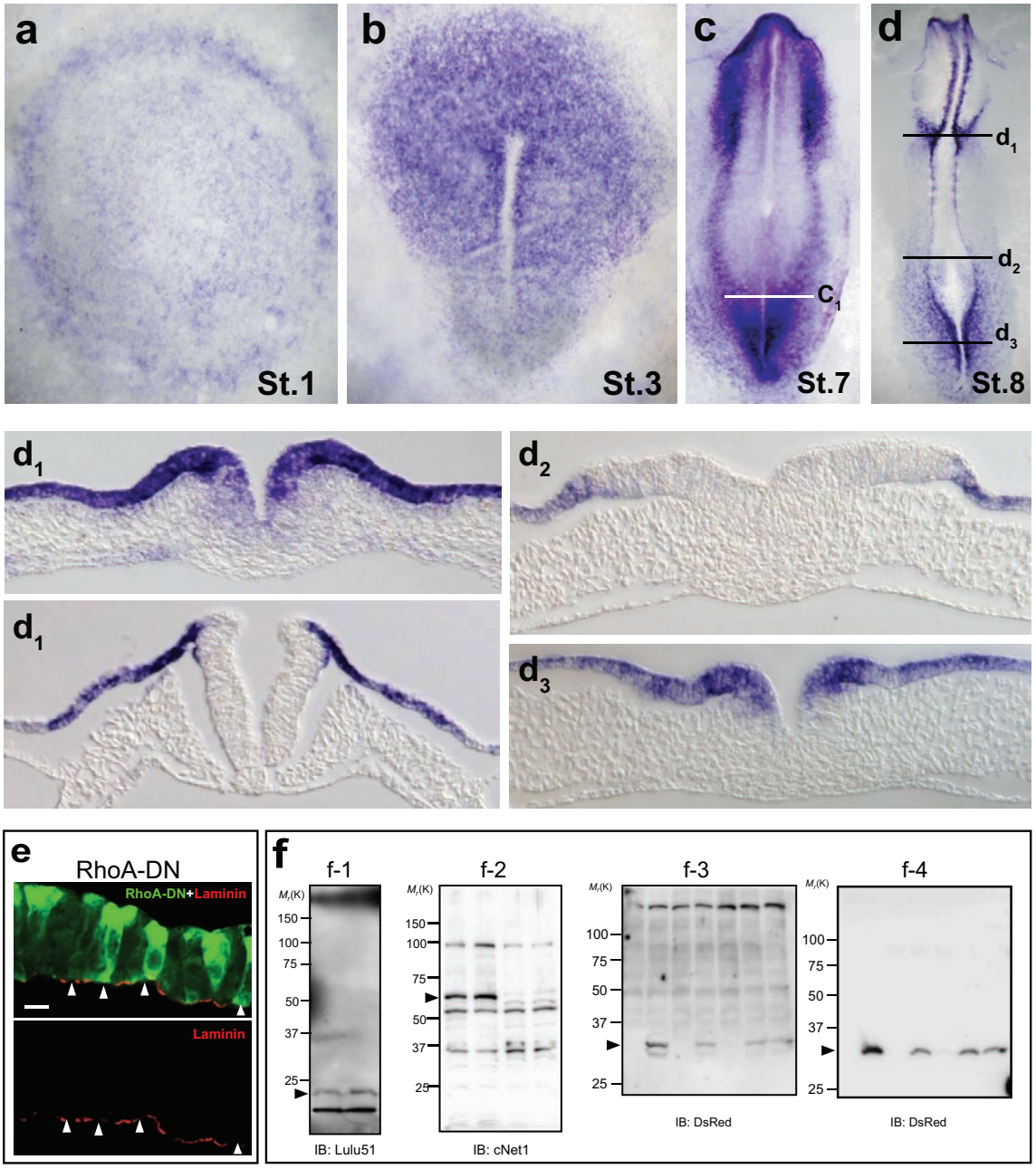

Figure S5 *Net1* in situ at additional stages, DN-RhoA effect and full-scan gels. *Net1* expression at pre-streak (**a**), HH3 (**b**), neural plate (**c**) and early somite (**d**) stages. Basal localisation of *Net1* transcripts is not seen at later stages ($\mathbf{c_1}$,$\mathbf{d_{1\text{-}3}}$). **e**: DN-RhoA causes BM-breakdown in lateral epiblast cells (arrowheads). Scale bar: 10 μm. **f**: Full-scan gels of those shown in Fig.S6g ($\mathbf{f_1}$), Fig.S6j ($\mathbf{f_2}$), Fig. S6k$_1$ ($\mathbf{f_3}$) and Fig.S6l$_1$ ($\mathbf{f_4}$) with specific detected bands indicated by arrowheads.

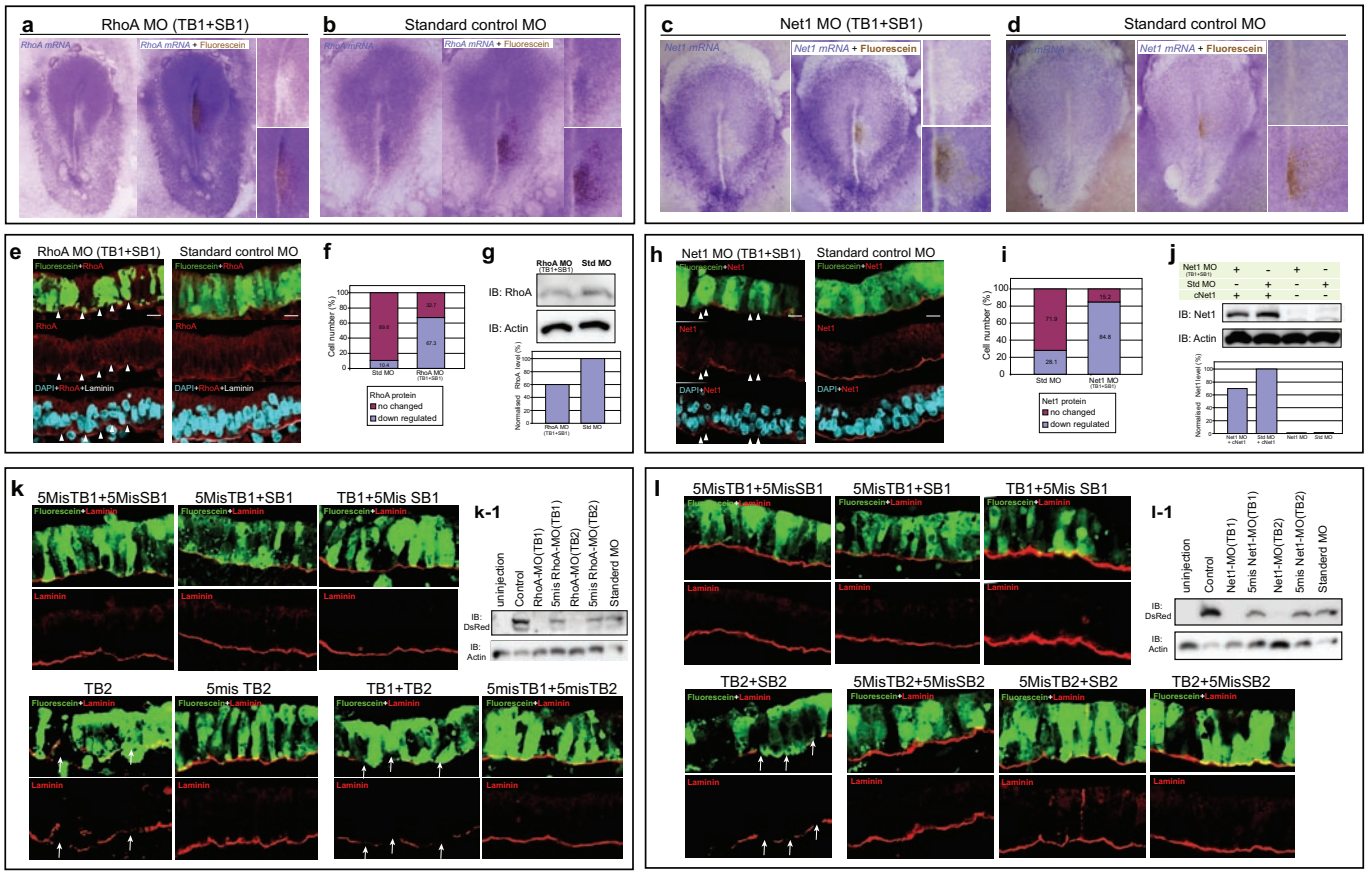

Figure S6 Specificity of *RhoA* and *Net1* morpholinos. Both *RhoA* MOs (TB1+SB1) **(a)** and *Net1* MOs (TB1+SB1) **(c)** can specifically reduce transcript levels. Standard control morpholinos do not affect transcript levels (**b** for *RhoA* and **d** for *Net1*). **e-g:** Effect of *RhoA* morpholinos on RhoA protein level is analysed by two methods. Immunohistochemical analysis (section in **e** and statistics in **f**) shows 67.3% *RhoA-MO* cells have reduced RhoA protein level (white arrowheads), compared to 10.4% seen with standard control MO cells. Alternatively, western blot of isolated epiblast tissue pieces electroporated with *RhoA-MOs* shows a 40% reduction compared to standard control MO electroporated tissue due to mosaic nature of epiblast cells receiving MOs. **h-j:** Effect of *Net1-MOs* on Net1 protein level. Immunohistochemical analysis (section in **h** and statistics in **i**) shows 84.8% *Net1-MO* cells have reduced Net1 protein level (white arrowheads), compared to 28.1% in standard control MO cells. Western blot of isolated epiblast tissue pieces electroporated with *Net1-MOs* and cNet1-expressing construct (endogenous Net1 expression is too low to be quantified in western blot) shows a 30% reduction compared to standard control. **k,l**: Additional MO (both specific and 5-mismatch control) experiments show MO specificity. Green: MOs. Red: laminin. **k**) Additional *RhoA-MOs*. Top panels: three combinations of 5-mismatch *RhoA* TB1 and SB1 MOs fail to cause BM-breakdown. Bottom panels: a second translation block MO (TB2) has a stronger effect, leading to potent BM-breakdown with TB2 alone or in combination with TB1; whereas its 5-mismatch controls do not. Specificity of translational block MOs is additionally demonstrated in *Xenopus* system (**k-1**) (see materials and methods). **l**) Additional *Net1* MOs. Top panels: three combinations of 5-mismatch *Net1* TB1 and SB1 MOs fail to cause BM-breakdown. Bottom panels: a similar specificity is seen with combination of two new *Net1* specific MOs (TB2+SB2); whereas their 5-mismatch controls fail to cause BM-breakdown. Specificity of *Net1* TB1 and TB2 MOs is additionally demonstrated in *Xenopus* system (**l-1**). Scale bar: 10 μm.

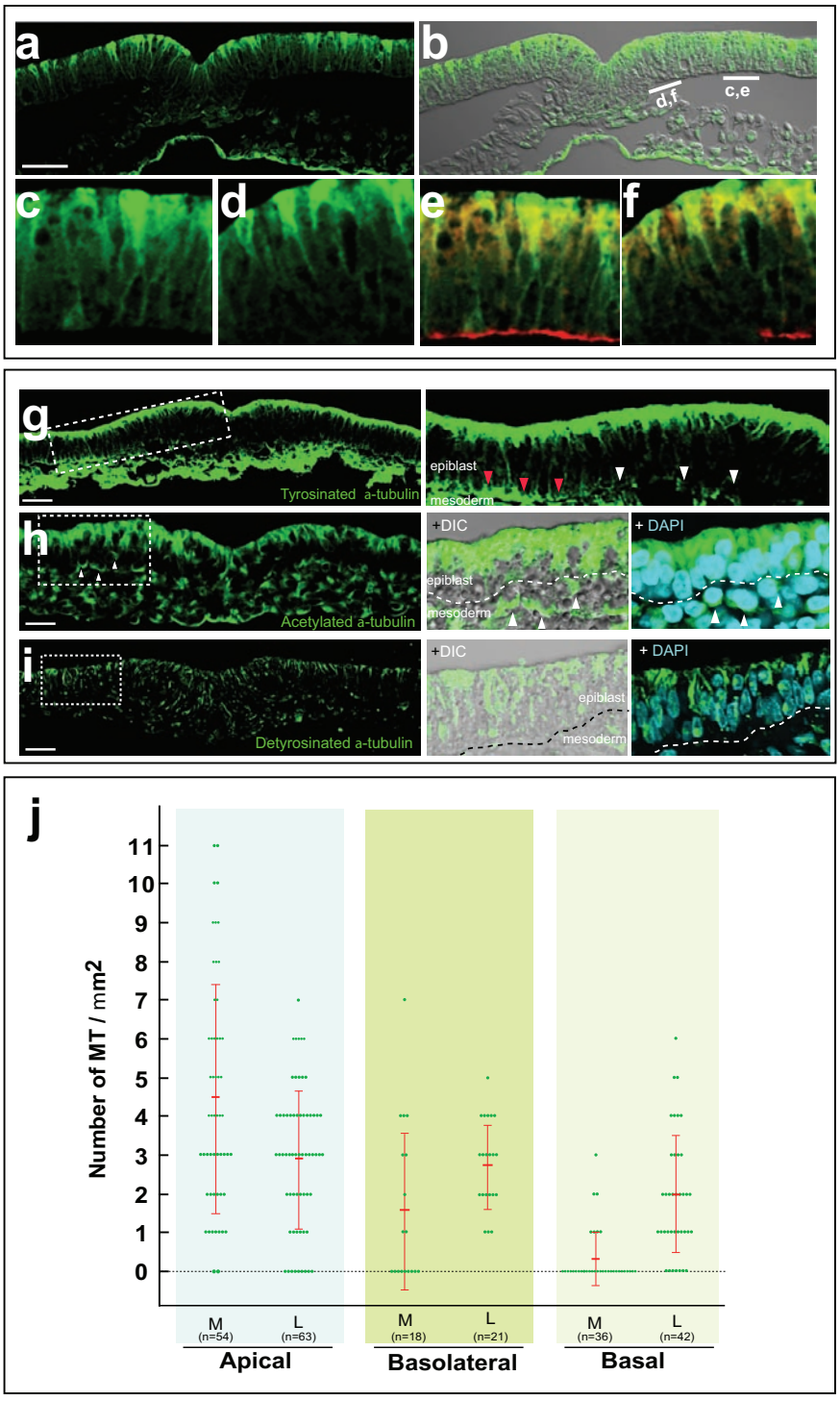

Figure S7 Tubulin staining and microtubule quantification. **a**-**f**: Mid-streak level section of HH4 embryo stained with pan-β-tubulin (**a**-**f**) and Laminin (**e**,**f**). Indicated regions in **b** are shown with high magnification in **c** and **d**. Co-staining with Laminin shows a similar loss of basal microtubules in medial epiblast cells (**e**,**f**). **g**-**i**: Immunofluorescence staining with antibodies against tyrosinated α-tubulin (**g**); acetylated α-tubulin (**h**) and detyrosinated α-tubulin (**i**). Right panel in **g** shows magnified view of indicated area on the left. Red arrowheads: basal staining in lateral epiblast cells. White arrowheads: lack of basal staining in medial epiblast cells. Right panels in **h** and **i** show a lack of basal staining, with DAPI-staining outlining the epiblast layer. White arrowheads in **h** indicate mesoderm staining. **j**: Numbers of microtubules per μm^2 are counted based on 80nm EM sections of a stage HH4 embryo. M: medial epiblast cells; L: lateral epiblast cells. Apical: apical third area. Basolateral: basal third but avoiding basal cortex. It is called basolateral here because central part of this region is often occupied by the nucleus. Basal: basal cortex area. Scale bar: 30 μm.

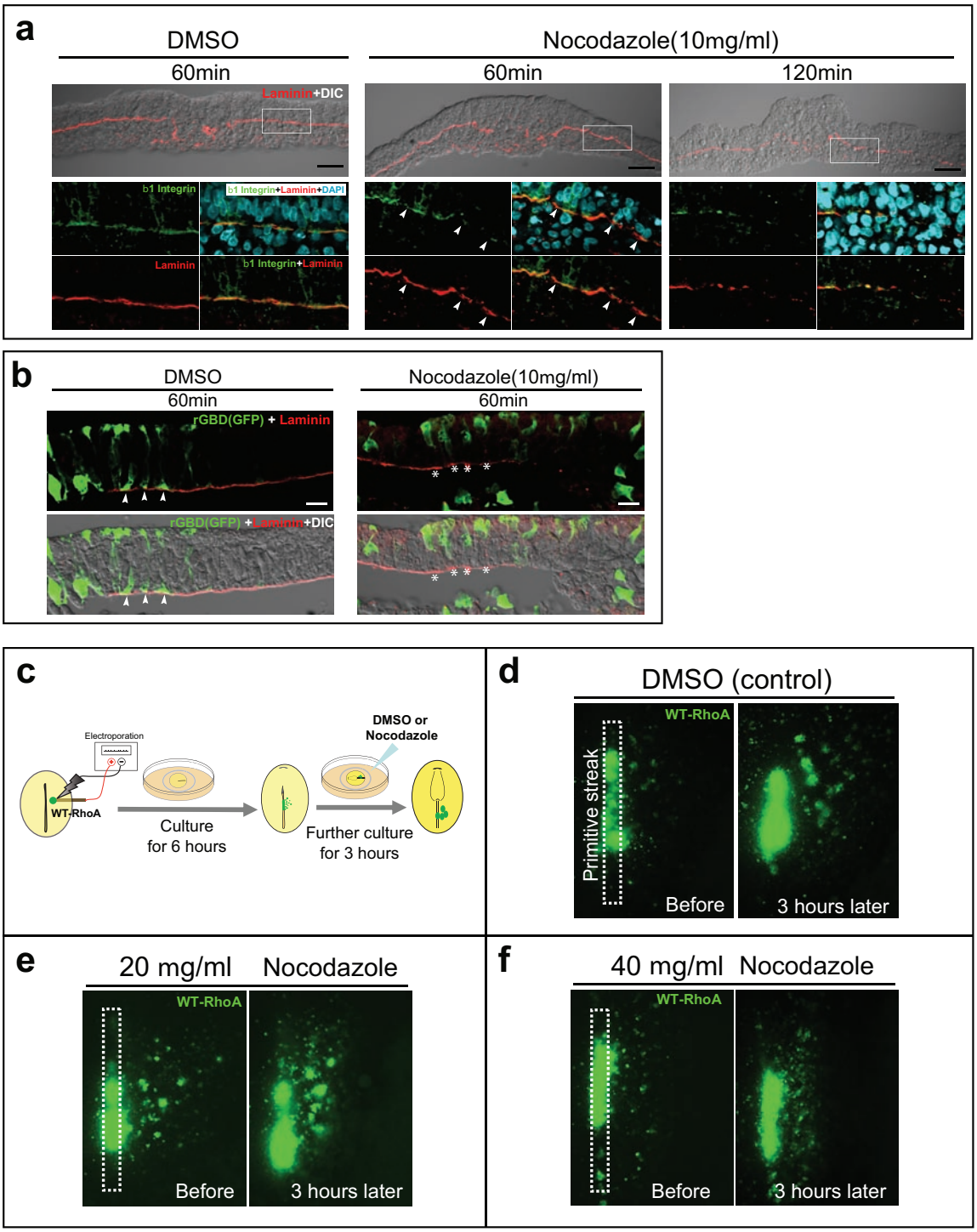

Figure S8 Effect of nocodazole treatment. **a,b**: Nocodazole effect on Laminin, integrin β1 and rGBD localization. **a)** 2 hour nocodazole treatment causes prominent loss of both laminin and integrin β1. 1 hour treatment causes less strong effect on both, but with more cells starting to lose integrin β1 than Laminin. White arrowheads indicate cells with intact Laminin but lost integrin β1 staining. **b)** rGBD distribution shows a more rapid response to nocodazole. White arrowheads: control treated cells retain basal rGBD signal. Asterisks: nocodazole treated cells lose basal rGBD signal. **c-f**: Nocodazole effect on RhoA caused cell aggregation. **c)** Schematic diagram of experimental procedure. **d)** Control treated embryo has prominent mesoderm cell aggregation. **e)** 20 μg/ml nocodazole treated embryo has some RhoA-expressing mesoderm cells migrating as individual cells, but still has aggregates formed. **f)** 40 μg/ml nocodazole treated embryo has most RhoA-expressing mesoderm cells migrating as individual cells. Scale bar: 30 μm (**a**); 10 μm (**b**).

Supplementary Movie Legends

Movie S1 Time-lapse movie (2-hour duration) of control GFP electroporated embryo.

Movie S2 Time-lapse movie (2-hour duration) of RhoA+GFP electroporated embryo.